NASA TECHNICAL MEMORANDUM 101672

THREE-DIMENSIONAL STRESS ANALYSIS OF PLAIN WEAVE COMPOSITES

John D. Whitcomb

November 1989

National Aeronautics and Space Administration
Langley Research Center
Hampton, Virginia 23665-5225

Abstract

Techniques were developed and described for performing three-dimensional finite element analysis of plain weave composites. This paper emphasizes aspects of the analysis which are different from analysis of traditional laminated composites, such as the mesh generation and representative unit cells. The analysis was used to study several different variations of plain weaves which illustrate the effects of tow waviness on composite moduli, Poisson's ratios, and internal strain distributions. In-plane moduli decreased almost linearly with increasing tow waviness. The tow waviness was shown to cause large normal and shear strain concentrations in composites subjected to uniaxial load. These strain concentrations may lead to earlier damage initiation than occurs in traditional cross-ply laminates.

Introduction

Traditionally, advanced composite structures have been fabricated from tape prepreg, which was stacked to form a laminate. This type of construction tends to give optimal in-plane stiffness and strength. Since the primary loads usually are in-plane, this fabrication procedure appeared logical. However, there are at least two reasons why the usual laminated construction may not be best. First, secondary loads due to load path eccentricities, impact, or local buckling can sometimes dominate the failure initiation because of the low through-thickness strength of traditional laminates. Second, for thick laminates there are many laminae which must be assembled. This results in tedious labor with many opportunities for mistakes in orienting the laminae.

Weaving is an alternate fabrication technique which has received considerable attention recently. The interlacing of fiber bundles in woven composites increases out-of-plane strength. Woven mats are thicker than a traditional lamina, hence fabrication of thick composites is less labor intensive and less prone to assembly error. These enhanced properties are obtained at the expense of some in-plane stiffness and strength. How much stiffness and strength is lost depends on the weave architecture. Because of the immense variety of possible weaves, it is not practical to determine optimal weave architecture through tests alone. Analytical models are needed which can predict the effect of various weave parameters on the mechanical properties.

Most of the analytical models which currently exist for woven composites were developed for prediction of moduli (eg. ref. 1, 2, 3). These models are based on many simplifying assumptions, similar to those found in classical laminate theory, which may be appropriate for moduli prediction, but which preempt the extension of the model for strength prediction. Models developed for stress analysis have generally been quasi-three-dimensional (Q3D) (ref. 4, 5). Since a Q3D analysis only models a single representative plane, little of the 3-D character of a woven composite is included. Ref. 2 includes some 3-D analysis, but the model was far too crude to permit stress analysis. Ref. 6 used a more refined 3-D finite element model than that in ref. 2, but the model was still probably not sufficiently refined for stress analysis (No stress distributions were reported.). There has been no detailed 3-D analysis of the stresses or strains in woven composites.

This paper has two objectives. The first objective is to describe a refined finite element based 3-D analysis of woven composites. Figure 1 shows a schematic of the repeating unit for a single mat of a plain weave composite, which is the particular woven form considered in this paper. The grid which overlays the tows in fig. 1 is there to clarify the geometry of the tows. The discussion of the analysis will emphasize aspects of the analysis which would be new to persons who have only analyzed conventional laminated composites. The second objective is to present a few results which illustrate the effect of tow waviness on the effective moduli, Poisson's ratios, and the internal strain distributions.

Symbols

C_{ijkl}	Constitutive coefficients
D	6 × 6 constitutive matrix
E_{11}, E_{22}, E_{33}	Young's moduli for orthotropic tow
$\bar{E}_x$, $\bar{E}_y$, $\bar{E}_z$	Average normalized Young's moduli for woven composite
F_x^i,F_y^i,F_z^i	Restraint forces in x-, y-, and z-directions, respectively, for load case i
G_{12}, G_{23}, G_{13}	Shear moduli for orthotropic tow
$\bar{G}_{xy}$, $\bar{G}_{yz}$, $\bar{G}_{xz}$	Average normalized shear moduli for woven composite
H	Half-thickness of finite element model
l_1, l_2	Half-lengths of wavy and straight parts of tow
P	Applied load in the x-direction
u, v, w	Displacements in x-, y-, and z-directions
u_o,v_o, w_o	Specified displacements in x-, y-, and z-directions
W	Half-width of finite element model ($W = l_1 + l_2$)
x, y, z	Cartesian coordinates
ε_x,ε_y,ε_z	Normal strains
ε_1, ε_2, ε_3, ε_{12}, ε_{23}, ε_{13}	Strains with respect to material coordinate system
ν_{12}, ν_{23}, ν_{13}	Poisson's ratios for orthotropic tow
$\bar{\nu}_{xy}$, $\bar{\nu}_{xz}$, $\bar{\nu}_{zy}$	Average normalized Poisson's ratios for woven composite

Analysis

Three-dimensional finite element analysis was used to study the behavior of plain weave composites. The finite element method was selected because of its flexibility in modeling complex shapes, spatial variation of material properties, and arbitrary boundary conditions. For moduli calculations a crude model can be used; for detailed stress analysis a much more refined model can be assembled, without any significant increase in professional manhours (compared to a crude model). In the following sections various aspects of the analysis will be discussed. First the configurations will be described, followed by sections on the finite element meshes and the material properties.

Configurations

The configurations analyzed consisted of mats of plain weave stacked to make a laminate. Figure 2 shows symmetric and unsymmetric stacking of the mats. The symmetry in fig. 2a is with respect to the interfaces between the mats.The geometry of an actual laminate is expected to be a complicated mix of these stackings. For this initial study the symmetric idealization in fig. 2a will be used. Such a laminate can be considered to be an assemblage of unit cells like that indicated in fig. 1. Because of symmetry within the unit cell, only one-fourth of the unit cell is actually modeled. Admittedly, this is a highly idealized plain weave composite. In actual composites the "synchrony" of the waviness in the mats could hardly be assured. Also, the interface between mats would not be planar. Furthermore, the shape of the tow cross-sections is likely to vary much more than is practical to model. In spite of the simplifications intrinsic

to the unit cell definition, this simplified cell definition is probably a reasonable starting point for detailed 3-D stress analysis. Fig. 3a shows a coarse finite element model of a plain weave. This model has a fairly small length of wavy tow (l_1) compared to the length of straight tow (l_2). Several different ratios of wavy to straight tows were considered. The ratio was varied by holding the length l_1 constant and varying l_2. The tow dimension H was also held constant. The term *waviness ratio* will be used as a measure of the fraction of tow which is inclined relative to the load direction. The waviness ratio is defined to be $l_1/(l_1 + l_2)$. Note that tow waviness varies inversely with tow width for a plain weave; narrow tows result in very wavy weaves.

Both extension and shear loadings were used. The boundary conditions for extension and shear were implemented quite differently, so they will be discussed separately. The dimensions and coordinate directions discussed below are defined in fig. 3a.

The boundary conditions for extension loads involve constraints on both displacements and net normal force on the same plane. Because of symmetry, there are no shear forces on the planes. Imposing a specific displacement (zero or non-zero) is a simple matter in finite element analysis (eg. specifying $u = 0$ on $x = -W$). Imposing a constraint on both displacements and forces on the same plane is much more complicated. For example, imposing the condition that $v = constant$ on $y = W$ and that the net restraint force is zero is not simple. Multi-point constraints could be imposed, but this is a complicated programming task and the number of nodes involved would result in a marked increase in the bandwidth of the equations. The approach taken herein is simple and does not affect the bandwidth. This approach, which is based on the principle of superposition, will be explained next by describing the steps required to obtain uniaxial loading of the unit cell in the x-direction. Because superposition is used, this approach is limited to linear analysis.

The first step is to impose normal constraints on all six faces of the finite element model.

$$\begin{aligned} &constrain\ u\ on\ x = \pm W \\ &constrain\ v\ on\ y = \pm W \\ &constrain\ w\ on\ z = \pm H \end{aligned} \tag{1}$$

A displacement $u = u_o$ is imposed on $x = W$ and the other constrained displacements are set to zero. The normal constraint forces are calculated for the three planes $x = W$, $y = W$, and $z = H$ and are defined to be F_x^1, F_y^1 and F_z^1, where the superscript indicates that these are forces from loading case one. The subscript indicates the direction of the force (and implicitly the plane on which the force acts). Next, a displacement $v = v_o$ is imposed on $y = W$ and the other constrained displacements are set to zero. The corresponding constraint forces F_x^2, F_y^2 and F_z^2 are determined. Finally, a displacement $w = w_o$ is imposed on $z = H$ and the other constrained displacements are set to zero. The corresponding constraint forces F_x^3, F_y^3 and F_z^3 are determined. These nine constraint forces are used in the following equations.

$$\begin{aligned} F_x^1 + aF_x^2 + bF_x^3 &= P \\ F_y^1 + aF_y^2 + bF_y^3 &= 0 \\ F_z^1 + aF_z^2 + bF_z^3 &= 0 \end{aligned} \tag{2}$$

The unknowns are the load in the x-direction ,P, and the scaling coefficients a and b. The last two equations express the condition that the net normal force on the $y = W$ and the $z = H$ planes must be zero. Solving the last two equations yields

$$b = \frac{-F_y^1 F_z^2 + F_z^1 F_y^2}{F_y^3 F_z^2 - F_z^3 F_y^2}$$
$$a = \frac{-F_y^1 - bF_Y^3}{F_Y^2} \tag{3}$$

These values of a and b can be used in equation (2) to determine the load. The average normal strains and two of the average Poisson's ratios are

$$\begin{aligned} \varepsilon_x &= \frac{u_o}{2W} \\ \varepsilon_y &= \frac{av_o}{2W} \\ \varepsilon_z &= \frac{bw_o}{2H} \\ \nu_{xy} &= -\frac{\varepsilon_y}{\varepsilon_x} \\ \nu_{xz} &= -\frac{\varepsilon_z}{\varepsilon_x} \end{aligned} \tag{4}$$

The effective Young's modulus in the x-direction $\bar{E}_x$ is calculated using the following energy balance equation

$$\frac{1}{2} P u_o = \frac{1}{2} \bar{E}_x \varepsilon_x^2 Vol \tag{5}$$

For the models considered in this paper one could have calculated $\bar{E}_x$ based on just the the average stress on the plane $x = W$ and the specified strain. In the more general case, the geometry might be such that there is no simple cross-sectional area which could be used to determine average stress. Such would be the case for the configuration in fig. 1 if the neat resin regions were left out.

The remaining Poisson's ratios and Young's moduli can be determined in a similar manner.

The exact boundary conditions for shear loading of an infinite array of unit cells require many multi-point constraints to impose anti-symmetry. Such boundary conditions permit the faces of the model to warp. The multi-point constraints complicate the analysis and significantly increase the computational cost. Hence, the approximate boundary conditions given below were used.

for G_{xy}:

$$u = ay \text{ and } v = ax \text{ on } x = \pm W \text{ and } y = \pm W \tag{6a}$$

for G_{yz}:

$$v = az \text{ and } w = ay \text{ on } y = \pm W \text{ and } z = \pm H \tag{6b}$$

for G_{xz}:

$$u = az \text{ and } w = ax \text{ on } x = \pm W \text{ and } z = \pm H \tag{6c}$$

These boundary conditions are very simple to impose. Consider the case of shear in the xy plane. Known non-zero displacements are prescribed on four faces. On $z = \pm H$ the displacement w is set to zero. This is posible because on the average, shear in the xy plane does not cause normal strain in the z-direction for the plain weave configuration studied herein. This is not generally true for textiles. For other material architectures a superposition procedure (like that described earlier) might be necessary.

Finite Element Meshes

Fig. 3 shows typical coarse and refined meshes for the plain weave composite. The coarse mesh had 595 nodes and 96 elements. The fine mesh had 3793 nodes and 768 elements. The elements were 20-node isoparametric hexahedrons. The meshes exhibit cyclic symmetry. In fact, a mesh is synthesized from the basic unit in fig. 4 rotated at 0^o, 90^o, 180^o, and 270^o about the z-axis.

In order to minimize the number of elements required, compatibility of displacements was not completely maintained at the center of the model. Fig. 5 illustrates the incompatability. Elements A and B are the same as those so labeled in fig. 3a. They are shown separated in fig. 5 to show the interface between the two elements and to show element C. There is some incompatability in the displacements because node 9 is not connected to any node in element A. However, since the resin material (eg. element A) is much more compliant than the tows, this approximation in the modeling is probably not significant. Even with the various simplifications, the internal shape of the mesh is fairly complicated. Work is needed to determine what refinements to the modeling would yield the greatest improvements in accuracy.

Some of the meshes had a larger ratio of wavy tow to straight tow than other meshes. Fig. 6 shows a mesh with a waviness ratio of .5, compared to a waviness ratio of .167 for the mesh in fig. 3.

Material Properties

The material properties chosen were for a hypothetical linear elastic graphite/epoxy composite. The tow properties were selected to be the same as for unidirectional tape prepreg material. The resin was assumed to be isotropic. The table below summarizes the assumed material properties.

	*Generic Graphite/Epoxy**	Neat Resin**
E_{11}	$13.4E10\ Pa$	$.345E10\ Pa$
E_{22}	$1.02E10\ Pa$	$.345E10\ Pa$
E_{33}	$1.02E10\ Pa$	$.345E10\ Pa$
ν_{12}	.3	.35
ν_{23}	.49	.35
ν_{13}	.3	.35
G_{12}	$.552E10\ Pa$	$.128E10\ Pa$
G_{23}	$.343E10\ Pa$	$.128E10\ Pa$
G_{13}	$.552E10\ Pa$	$.128E10\ Pa$

*ref. 7
**ref. 8

There are two angles which describe the orientation of a tow at any point. There is a primary rotation about the z-axis of either 0^o or 90^0. This angle is constant for a particular tow. There is also a secondary rotation about the x- or y-axis due to the waviness. The amount of rotation about the x- and y-axes varies spatially. This second rotation was determined based on the direction of the normal to the surface defined by four of the midside nodes, which are labeled a, b, c, and d in fig. 7. The surface normal direction was calculated as the cross product $\mathbf{N} = \mathbf{ca} \times \mathbf{db}$. Appendix A describes the material property transformations required because of these rotations. A right-handed coordinate system is assumed. Positive rotations are defined to be counterclockwise from the material axis to the global axis (or clockwise from the global axis to the material axis).

Results and Discussion

Several configurations were analyzed to determine the effect of tow waviness on effective moduli, Poisson's ratios, and internal strain distributions. The results of these analyses will be discussed in this section.

Figs. 8a and 8b show the effect of tow waviness on the effective moduli and three of the Poisson's ratios. The properties are normalized by those for a conventional $(0/90)_s$ laminate fabricated from tape material. For reference, the properties for a $(0/90)_s$ laminate are listed below.

$$E_x = 7.25E10Pa \qquad E_z = 1.27E10\ Pa$$
$$G_{xy} = .552E10\ Pa \qquad G_{yz} = .426E10\ Pa$$
$$\nu_{xy} = .0424 \qquad \nu_{zy} = .0795 \qquad \nu_{xz} = .455$$

Most of the results were generated using coarse models. A few results were generated using refined models. The differences in the moduli for the coarse and fine models were insignifcant, so only the results for the coarse mesh are shown in fig. 8a. There was more difference between the coarse and fine models for the Poisson's ratios. Hence, results for both model refinements are shown in fig. 8b. The solid lines are the results for the coarse model. The solid circles are the results for the fine model.

Fig. 8a shows that $\bar{E}_x$, $\bar{E}_z$ and $\bar{G}_{xy}$ decrease almost linearly with increased waviness. The waviness has the largest effect on $\bar{E}_x$. Some of the decrease can be attributed to the increase in resin content as waviness increases. The volume of neat resin pockets increases from 3.2 percent for the case with a waviness ratio of .167 to 12.5 percent for the case with a waviness ratio of .5 . The transverse shear modulus $\bar{G}_{yz}$ increases with increased waviness. Fig. 8b shows that the in-plane Poisson's ratio $\bar{\nu}_{xy}$ decreases with increased waviness. The other two Poisson's ratios $\bar{\nu}_{xz}$ and $\bar{\nu}_{zy}$ increase with waviness. The variation is essentially linear. There is more difference between the results for the coarse and refined models for large waviness than for small waviness. Numerical values of the coarse model results in fig. 8 are tabulated in Table 1.

No experiments were performed as part of this study, but some qualitative comparisons can be made with the results in ref. 9. Ref. 9 presents analytical and experimental in-plane modulus results for a plain weave, oxford weave, 5 harness satin weave, and an 8 harness satin weave. No results were presented for a (0/90/90/0) tape laminate, but the 8 harness satin results should have close to the same moduli, since it has low waviness. The loss in axial stiffness $\bar{E}_x$ shown in fig. 8 agrees qualitatively with ref. 9. Fig. 8 shows a decrease in $\bar{\nu}_{xy}$ with increased waviness, but the analytical results in ref. 9 predicts no change and the experiments showed an increase. Fig. 8 shows a decrease in $\bar{G}_{xy}$ with increased waviness, which agrees with the experimental results in ref. 9, but which disagrees with the analytical results. There is obviously a need for further analytical and experimental work to clarify the source of these inconsistencies.

Strain distributions were calculated for weaves with waviness ratios of .167 and .5. Refined finite element meshes were used. The procedure for smoothing the strains to obtain nodal strains is described in Appendix B. Because of limited space, only a few of the results will be presented here. Also, only uniaxial loading was considered for the results herein. The results will be presented in terms of isostrain contours. The strains are normalized by the magnitude of the applied axial strain. These strains are calculated relative to the material coordinate system, in which the x_1-axis is along the tow direction, the x_2-axis is in-plane and perpendicular to the x_1-axis, and the x_3-axis is perpendicular to the other two axes. Since no convergence study was performed, the results should be considered qualitative.

For the case with a waviness ratio of .167, fig. 9 shows the 0^o tow for which strain contours will be presented. Fig. 10 identifies the analogous area for the case with a waviness ratio of .5. The area in fig. 10 labeled ABCD is identical in geometry to the area labeled ABCD in fig. 9.

Hence, the only difference between the two models is the straight-tow region in the mesh with the smaller waviness ratio.

Fig. 11 shows contours of constant ε_1 for the case with a waviness ratio of .167. The largest strain concentration is at (x,y,z)=(0,0,0). There are strong, fairly complicated strain gradients near (x,y,z)=(0,0,0), but a few tow thicknesses away from the y=0 plane, the variation in strain on any $y = y_o$ plane is independent of y_o. A two-dimensional analysis would probably do a reasonable job in the region away from the $y = 0$ plane, but obviously could not predict the peak strains, which occur near the origin.

Figures 12a-12f show ε_1, ε_2, ε_3, ε_{12}, ε_{23}, and ε_{13} contours for the region labeled ABCD in fig. 11. As just mentioned, the largest ε_1 occurs at the origin. The magnitude there is approximately 2.7 times the average strain for the unit cell. This strain concentration would be expected to cause fiber breakage at a lower global strain than would occur in a tape laminate. Much of the strain concentration is likely due to tapering of the tow in both the x- and y-directions to a zero thickness at the origin (see fig. 4). Herein lies a particularly sticky modeling problem. Even though the tow cross section may actually vary as indicated by the finite element model, the tapering is due to migration,not termination, of the individual fibers. That is, fibers near the $y = 0$ plane which are aligned parallel to the x-axis away from the origin are squeezed further away from the $y = 0$ plane as they approach the origin, resulting in a zero tow thickness at the origin. This fiber migration causes a very complicated variation in the local constitutive properties of the tow. There was no attempt in this paper to account for this. The straightening of the tow under tensile loads causes an increase in ε_1 at point E and a decrease in ε_1 at point F.

Fig. 12b shows that the ε_2 strains are small. The peak magnitude occurs on the $y = 0$ plane, probably because that is the boundary of the tow, where there is an abrupt change in local properties.

Fig. 12c shows that both the magnitude and variation of ε_3 are large. The presence of large ε_3 strains has been previously reported in ref. (4). In that study a quasi-3D analysis was used. Fig. 12c shows that the strain variation is nearly 2D in character, except where the peak occurs. The large magnitude of ε_3 might cause delamination.

A uniaxially-loaded conventional $(0/90)_s$ laminate fabricated from tape prepreg has no shear strains away from free edges. Figs. 12d-12f show that a plain weave fabric has significant shear strains. The peak ε_{12} is about the same magnitude as the average axial strain. Particularly under fatigue loading, the ε_{12} could lead to intra-tow cracking. The peak ε_{23} (fig. 12e) is also nearly as large as the average axial strain. The peak occurs along the tow boundary and might lead to some inter-tow cracking, particularly under fatigue.

The ε_{13} strain component (fig. 12f) is by far the largest strain component. This strain component is due to the eccentricity of the two ends of the tow. The very large magnitude suggests that delamination initiation might be dominated by this strain component.

The strain contours for the case with a waviness ratio of .5 are very similar to those in fig. 12. The contours for ε_1 and ε_{13} are shown in fig. 13 to illustrate the similarity. Interestingly, the peak strains tend to be larger for the less wavy weave for the same average axial strain. Table 2 lists the minimum and maximum strains for the two weaves. However, the less wavy weave also has a higher axial stiffness. For a given average strain the average stress is higher for the less wavy weave. If both weaves are subjected to the same average stress, the peak strains in the more wavy weave are about as large or larger than for the less wavy weave, which is more in line with intuition.

Conclusions

Techniques were developed and described for performing three-dimensional finite element analysis of plain weave composites. The discussion of the analysis emphasized aspects of the

analysis which are different from analysis of traditional laminated composites, such as mesh generation and representative unit cells.

The analysis was used to study several different weaves to determine the effects of tow waviness on composite moduli, Poisson's ratios, and internal strain distributions. The average normalized composite moduli $\bar{E}_x$, $\bar{G}_{xy}$, and $\bar{E}_z$ all decreased with increasing waviness. The average normalized out-of-plane shear modulus $\bar{G}_{xz}$ increased with increasing waviness. As expected, there are significant strain gradients. The magnitude of these strain concentrations suggest that damage initiation will occur at a significantly lower global strain than for a traditional cross-ply laminate. However, some of the most severe strain concentrations occur where the weave geometry is most difficult to model with confidence. Experimental work is needed to characterize the variation of the fiber tow geometry and to document the initiation of damage under static and fatigue loads.

NASA Langley Research Center
Hampton, VA 23665-5225
November , 1989

Appendix A
Material Property Transformations

This appendix describes the material property transformations which are required between the global and material coordinate systems. Transformations from one coordinate system to another are needed for strains, stresses, and the material properties. Although the finite element analysis calculates the strains and stresses relative to the global coordinate system, it is reasonable to report them relative to the material coordinate system. The material properties are known relative to the material coordinate system, but the finite element formulation requires the properties relative to the global coordinate system. Hence, there are transformations in "both directions".

To obtain the strains with respect to the material coordinate axes requires a second order tensor transformation. The transformation rule between the global and material coordinate systems is given by (ref. 10)

$$\varepsilon'_{ij} = a_{im} a_{jn} \varepsilon_{mn} \tag{A1}$$

where the ε'_{ij} are the strains in the material coordinate system and a_{ij} = cosine of angle between the x'_i and x_j axes which are the material coordinate axes and the global coordinate axes, respectively. Fig. A1 illustrates the definition of the a_{ij} for a rotation about the z-axis only.

In expanded form, eqn. (A1) can be written as

$$\begin{bmatrix} \varepsilon'_{11} \\ \varepsilon'_{22} \\ \varepsilon'_{33} \\ \varepsilon'_{12} \\ \varepsilon'_{21} \\ \varepsilon'_{23} \\ \varepsilon'_{32} \\ \varepsilon'_{13} \\ \varepsilon'_{31} \end{bmatrix} = [T_1] \begin{bmatrix} \varepsilon_{11} \\ \varepsilon_{22} \\ \varepsilon_{33} \\ \varepsilon_{12} \\ \varepsilon_{21} \\ \varepsilon_{23} \\ \varepsilon_{32} \\ \varepsilon_{13} \\ \varepsilon_{31} \end{bmatrix} \tag{A2}$$

where

$$[T_1] = \begin{bmatrix} a_{11}a_{11} & a_{12}a_{12} & a_{13}a_{13} & a_{11}a_{12} & a_{12}a_{11} & a_{12}a_{13} & a_{13}a_{12} & a_{11}a_{13} & a_{13}a_{11} \\ a_{21}a_{21} & a_{22}a_{22} & a_{23}a_{23} & a_{21}a_{22} & a_{22}a_{21} & a_{22}a_{23} & a_{23}a_{22} & a_{21}a_{23} & a_{23}a_{21} \\ a_{31}a_{31} & a_{32}a_{32} & a_{33}a_{33} & a_{31}a_{32} & a_{32}a_{31} & a_{32}a_{33} & a_{33}a_{32} & a_{31}a_{33} & a_{33}a_{31} \\ a_{11}a_{21} & a_{12}a_{22} & a_{13}a_{23} & a_{11}a_{22} & a_{12}a_{21} & a_{12}a_{23} & a_{13}a_{22} & a_{11}a_{23} & a_{13}a_{21} \\ a_{21}a_{11} & a_{22}a_{12} & a_{23}a_{13} & a_{21}a_{12} & a_{22}a_{11} & a_{22}a_{13} & a_{23}a_{12} & a_{21}a_{13} & a_{23}a_{11} \\ a_{21}a_{31} & a_{22}a_{32} & a_{23}a_{33} & a_{21}a_{32} & a_{22}a_{31} & a_{22}a_{33} & a_{23}a_{32} & a_{21}a_{33} & a_{23}a_{31} \\ a_{31}a_{21} & a_{32}a_{22} & a_{33}a_{23} & a_{31}a_{22} & a_{32}a_{21} & a_{32}a_{23} & a_{33}a_{22} & a_{31}a_{23} & a_{33}a_{21} \\ a_{11}a_{31} & a_{12}a_{32} & a_{13}a_{33} & a_{11}a_{32} & a_{12}a_{31} & a_{12}a_{33} & a_{13}a_{32} & a_{11}a_{33} & a_{13}a_{31} \\ a_{31}a_{11} & a_{32}a_{12} & a_{33}a_{13} & a_{31}a_{12} & a_{32}a_{11} & a_{32}a_{13} & a_{33}a_{12} & a_{31}a_{13} & a_{33}a_{11} \end{bmatrix}$$

Assuming the strain tensor is symmetric ($\varepsilon_{ij} = \varepsilon_{ji}$), and performing trivial modification gives the transformation in terms of the engineering shear strains, which are 2× the tensor shear strains.

$$\begin{bmatrix} \varepsilon'_{11} \\ \varepsilon'_{22} \\ \varepsilon'_{33} \\ 2\varepsilon'_{12} \\ 2\varepsilon'_{23} \\ 2\varepsilon'_{13} \end{bmatrix} = [T_2] \begin{bmatrix} \varepsilon_{11} \\ \varepsilon_{22} \\ \varepsilon_{33} \\ 2\varepsilon_{12} \\ 2\varepsilon_{23} \\ 2\varepsilon_{13} \end{bmatrix} \tag{A3}$$

where

$$[T_2] = \begin{bmatrix} a_{11}a_{11} & a_{12}a_{12} & a_{13}a_{13} & 2a_{11}a_{12} & 2a_{12}a_{13} & 2a_{11}a_{13} \\ a_{21}a_{21} & a_{22}a_{22} & a_{23}a_{23} & 2a_{21}a_{22} & 2a_{22}a_{23} & 2a_{21}a_{23} \\ a_{31}a_{31} & a_{32}a_{32} & a_{33}a_{33} & 2a_{31}a_{32} & 2a_{32}a_{33} & 2a_{31}a_{33} \\ a_{11}a_{21} & a_{12}a_{22} & a_{13}a_{23} & a_{11}a_{22}+a_{12}a_{21} & a_{12}a_{23}+a_{13}a_{22} & a_{11}a_{23}+a_{13}a_{21} \\ a_{21}a_{31} & a_{22}a_{32} & a_{23}a_{33} & a_{21}a_{32}+a_{22}a_{31} & a_{22}a_{33}+a_{23}a_{32} & a_{21}a_{33}+a_{23}a_{31} \\ a_{11}a_{31} & a_{12}a_{32} & a_{13}a_{33} & a_{11}a_{32}+a_{12}a_{31} & a_{12}a_{33}+a_{13}a_{32} & a_{11}a_{33}+a_{13}a_{31} \end{bmatrix}$$

Stress is also a second order tensor, so the transformation is the same as for the tensor strains (eqns. (A1) and (A2)). Since there is no distinction between engineering and shear stresses, the further manipulations resulting in eqn.(A3) are not applicable.

The material properties are ordinarily defined with respect to the material coordinate axes, but the finite element formulation requires that they be defined with respect to the global coordinate axes. The material constitutive coefficients comprise a fourth order tensor. Hence, the form of the transformation rule is (ref. 10)

$$C_{ijkl} = a_{im}a_{jn}a_{ko}a_{lp}C'_{mnop} \tag{A4}$$

Note that the a_{ij} in eqn. (A4) are different than those in eqn. (A1), since the transformation is in the opposite direction (ie. from the material axes to the global axes).

Eqn. (A4) is cumbersome. Alternately, we can derive a matrix form of the transformation based on the invariance of the strain-energy density. Also, this alternate transformation makes use of the already calculated matrix T_2. The invariance can be expressed as

$$\underline{\varepsilon}^T D\varepsilon = \underline{\varepsilon}'^T D'\underline{\varepsilon}' \tag{A5}$$

where

$$\underline{\varepsilon} = \begin{bmatrix} \varepsilon_{11} \\ \varepsilon_{22} \\ \varepsilon_{33} \\ 2\varepsilon_{12} \\ 2\varepsilon_{23} \\ 2\varepsilon_{13} \end{bmatrix}$$

and D is a 6×6 constitutive matrix.

Eqns. (3) and (5) can be combined to obtain

$$\underline{\varepsilon}^T D\varepsilon = \underline{\varepsilon}^T T_2^T D' T_2 \varepsilon \tag{A6}$$

From eqn. (A6) it is obvious that the transformation rule is

$$D = T_2^T D' T_2 \tag{A7}$$

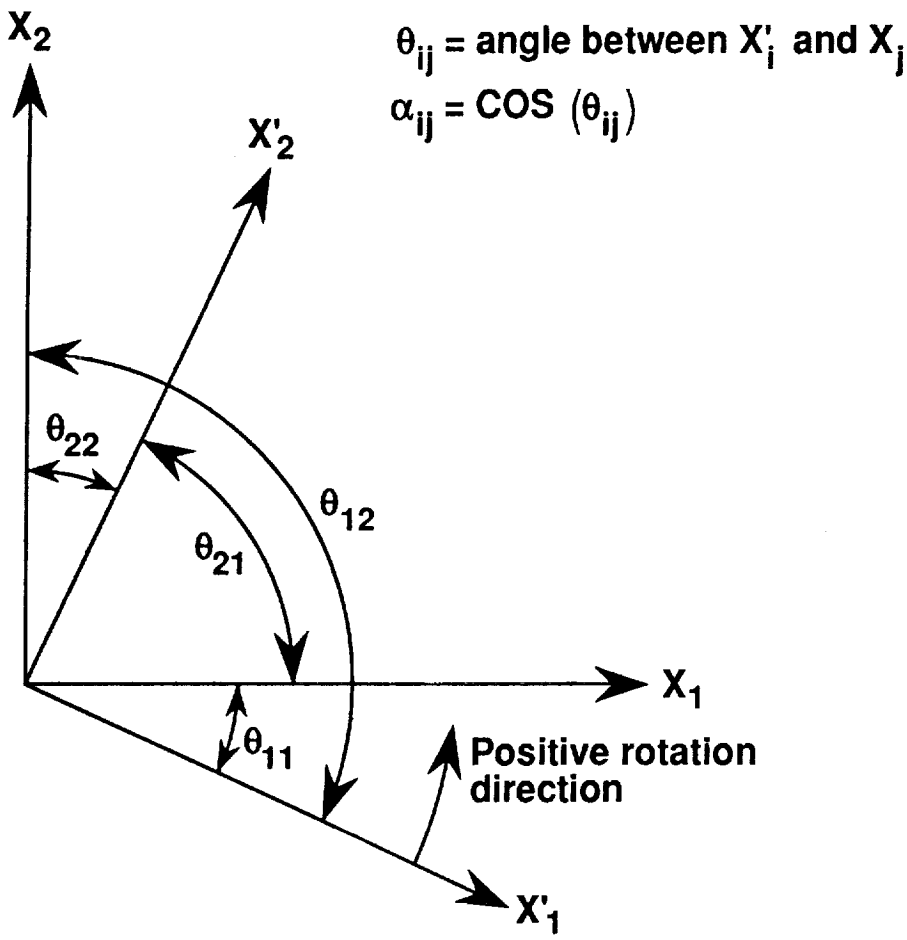

Figure A1. Definition of a_{ij} for rotation about x_3 axis.

Appendix B

Strain Smoothing

This appendix describes the procedure used to smooth the strains. The smoothing procedure calculates nodal strains based on the strains calculated at the quadrature points. The procedure is based on ref. 11. It is assumed that strains are available at 8 quadrature points. The ordering of the terms in the matrices which will be described depends on the numbering sequence for the corner nodes in a single element and the quadrature points. Fig. B1 shows the numbering sequence for the nodes and the quadrature points. For clarity in the sketch, some nodes and quadrature points are not shown. However, the numbering patterns for the hidden nodes and points are the same as for those shown.

The smoothing procedure begins with assuming a functional form for the strains within an element. The form assumed herein is

$$\begin{aligned} &\varepsilon(x_1,x_2,x_3) = S^i(x_1,x_2,x_3)C^i \quad sum\ on\ i \\ &where\ [S^i] = [1\ \ x_1\ \ x_2\ \ x_3\ \ x_1x_2\ \ x_1x_3\ \ x_2x_3\ \ x_1x_2x_3] \end{aligned} \tag{B1}$$

Equation (B1) can be written for the 8 quadrature points in the following form:

$$[\varepsilon] = \begin{bmatrix} 1 & -A & -A & -A & B & B & B & -C \\ 1 & -A & -A & A & B & -B & -B & C \\ 1 & -A & A & -A & -B & -B & B & C \\ 1 & -A & A & A & -B & B & -B & -C \\ 1 & A & -A & -A & -B & B & -B & C \\ 1 & A & -A & A & -B & -B & B & -C \\ 1 & A & A & -A & B & -B & -B & -C \\ 1 & A & A & A & B & B & B & C \end{bmatrix} \begin{bmatrix} C^1 \\ C^2 \\ C^3 \\ C^4 \\ C^5 \\ C^6 \\ C^7 \\ C^8 \end{bmatrix} \tag{B2}$$

where $A = 1/\sqrt{3}$, $B = 1/3$, and $C = A * B$

Equation B2 can be solved for the coefficients C^i.

$$[C^i] = [H]^{-1}[\varepsilon^i] \tag{B3}$$

where H is the coefficient matrix in equation B2.

With the C^i known, the strains at the nodes can be determined using equation (B1). The smoothing procedure can be summarized in terms of a single matrix multiplication.

$$[\varepsilon^i_n] = [T][\varepsilon^i_q] \tag{B4}$$

where the subscripts n and q indicate nodal or quadrature values, respectively and the matrix $[T]$ is

$$\begin{bmatrix} A & B & B & C & B & C & C & D \\ B & C & A & B & C & D & B & C \\ C & B & B & A & D & C & C & B \\ B & A & C & B & C & B & D & C \\ B & C & C & D & A & B & B & C \\ C & D & B & C & B & C & A & B \\ D & C & C & B & C & B & B & A \\ C & B & D & C & B & A & C & B \end{bmatrix} \tag{B5}$$

where

$$A = 5 + 3 * E$$
$$D = 5 - 3 * E$$
$$B = -1 - E$$
$$C = -1 + E$$
$$where\ E = \sqrt{3}$$

This procedure gives the nodal strains for an individual element. Most nodes in a mesh are shared by several elements. A simple averaging procedure was used to smooth discontinuities in the strain field. Since strain discontinuities are physically possible at bimaterial interfaces, the averaging was performed among elements of the same material type. This averaging procedure must be performed before transforming the strains to the material coordinate system.

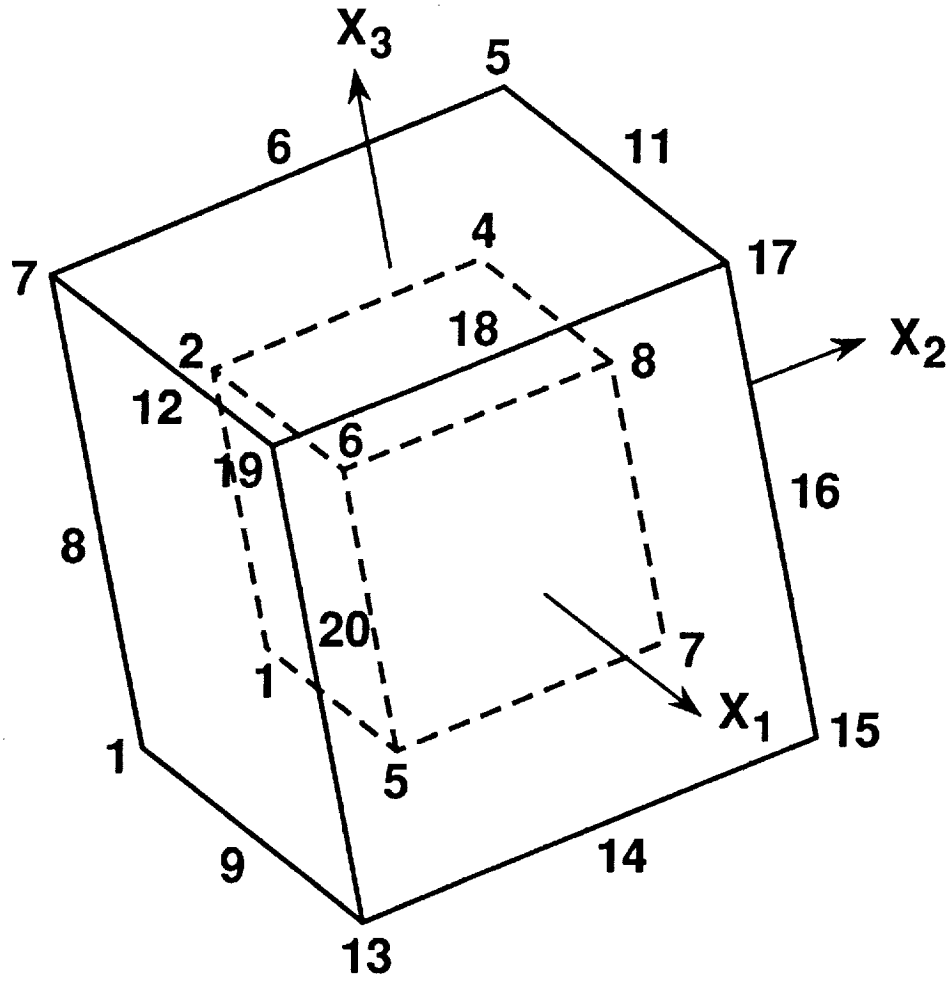

Figure B1. Numbering sequence for nodes and quadrature points.

References

1. Halpin, J. C.; Jerine, K.; and Whitney, J. M.: The Laminate Analogy for 2 and 3 Dimensional Composite Materials. Journal of Composite Materials, Vol. 5, Jan. 1971, pp. 36-49.
2. Ishikawa, T.: Anti-Symmetric Elastic Properties of Composite Plates of Satin Weave Cloth. Fibre Science and Technology, Vol. 15, 1981, pp. 127-145.
3. Ishikawa, T. and Chou, T. W.: Stiffness and Strength Behavior of Woven Fabric Composites. Journal of Material Science, Vol. 17, 1982, pp. 3211-3220.
4. Avery, W. B. and Herakovich, C. T.: A Study of the Mechanical Behavior of a 2-D Carbon-Carbon Composite. Virginia Polytechnic Institute and State University Report VPI-E-87-15 or CCMS-87-13, August, 1987.
5. Kriz, R. D. : Influence of Damage on Mechanical Properties of Woven Composites at Low Temperatures. Journal of Composite Technology & Research, Vol. 7, No. 2, Summer 1985, pp. 55-58.
6. Dow, N. F. and Ramnath, V.: Analysis of Woven Fabrics for Reinforced Composite Materials. NASA Contract Report 178275, April, 1987.
7. Wang, S. S. and Choi, I.: The Mechanics of Delamination in Fibre-reinforced Composite Laminates. Part I- Stress Singularities and Solution Structure. Part II- Delamination Behavior and Fracture Mechanics Parameters. NASA CR 172269 and CR 172270, Nov. 1983.
8. Halpin, J. C. : Primer on Composite Materials: Analysis. Technomic Publishing Co., Inc. Lancaster, 1984, p. 166.
9. Foye, R. L.: The Mechanics of Fabric-Reinforced Composites. Proceedings of Fiber-Tex Conference, Sept., 1988. NASA Conference Publication 3038, pp. 237-247.
10. Frederick, D. and Chang, T. S.: Continuum Mechanics. Scientific Publishers, Inc., Cambridge, 1972, p. 29
11. Hinton, E.; Scott, F. C.; and Ricketts, R. E.: Local Least Squares Stress Smoothing for Parabolic Isoparametric Elements. International Journal for Numerical Methods in Engineering, vol. 9, pp. 235-256, 1975.

Table 1. Effect of Waviness on Moduli and Poisson's Ratios
(Coarse Mesh Results)

	Waviness Ratio		
	.167	.25	.5
$\bar{E}_x$	.92	.88	.75
$\bar{E}_z$	.95	.93	.84
$\bar{G}_{xy}$	.96	.94	.87
$\bar{G}_{yz}$	1.10	1.14	1.22
$\bar{\nu}_{xy}$	.87	.81	.60
$\bar{\nu}_{zy}$	1.14	1.21	1.45
$\bar{\nu}_{xz}$	1.10	1.14	1.28

Table 2. Maximum Normalized Strains for Waviness Ratios of .167 and .5

Normalized Strain*	Waviness Ratio = .167		Waviness Ratio = .5	
	Min.	Max.	Min.	Max.
$\bar{\varepsilon}_1$	.44	2.7	.35	2.2
$\bar{\varepsilon}_2$	−.42	.29	−.32	.27
$\bar{\varepsilon}_3$	−1.4	1.6	−1.4	1.2
$\bar{\varepsilon}_{12}$	−1.0	1.0	−.82	.82
$\bar{\varepsilon}_{23}$	−.83	.83	−.68	.68
$\bar{\varepsilon}_{13}$	−3.4	3.4	−2.9	2.9

*Normalized Strain = Strain/Specified Axial Strain

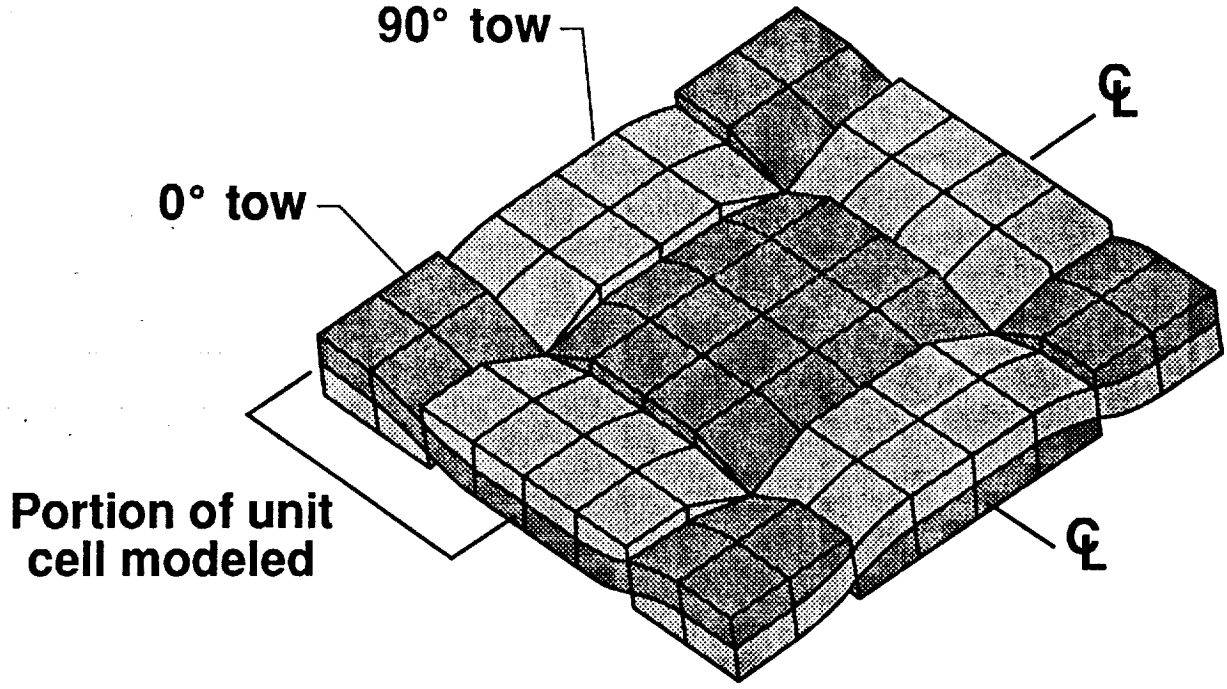

Figure 1. Schematic of plain weave unit cell. (Neat resin regions removed to show tow structure.)

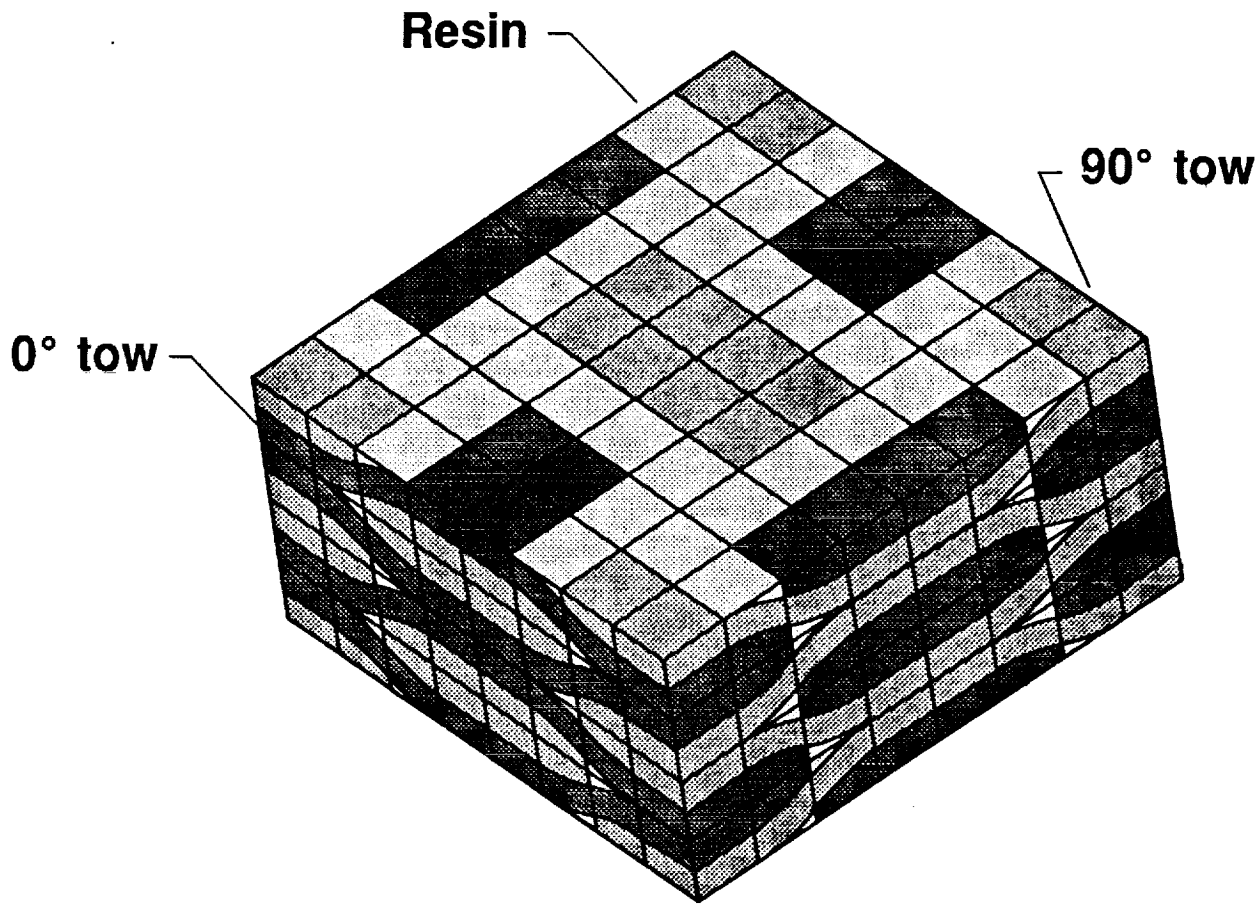

(a) Symmetric stacking

Figure 2. Stacking of plain weave mats.

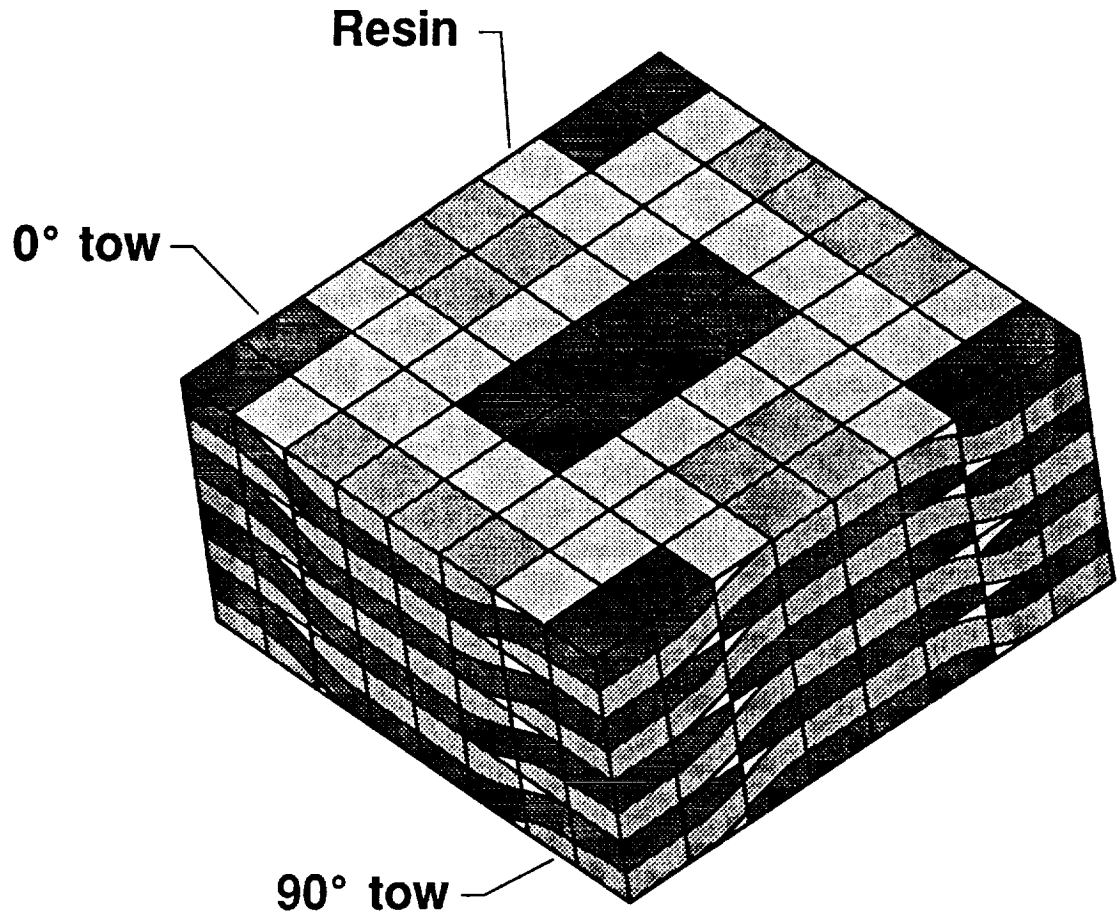

(b) Unsymmetric stacking

Figure 2. Concluded.

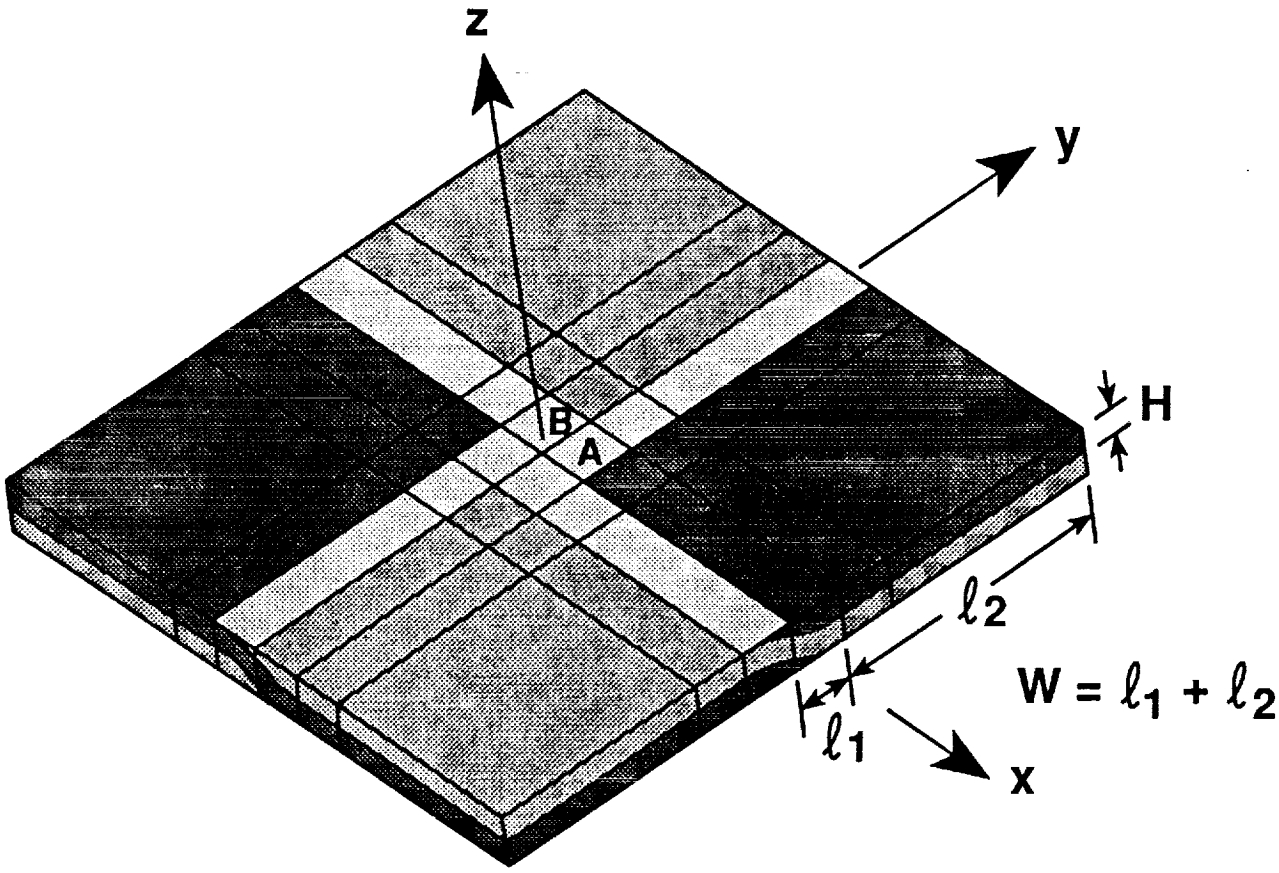

(a) Coarse mesh (595 nodes, 96 elements)

Figure 3. Typical finite element meshes.

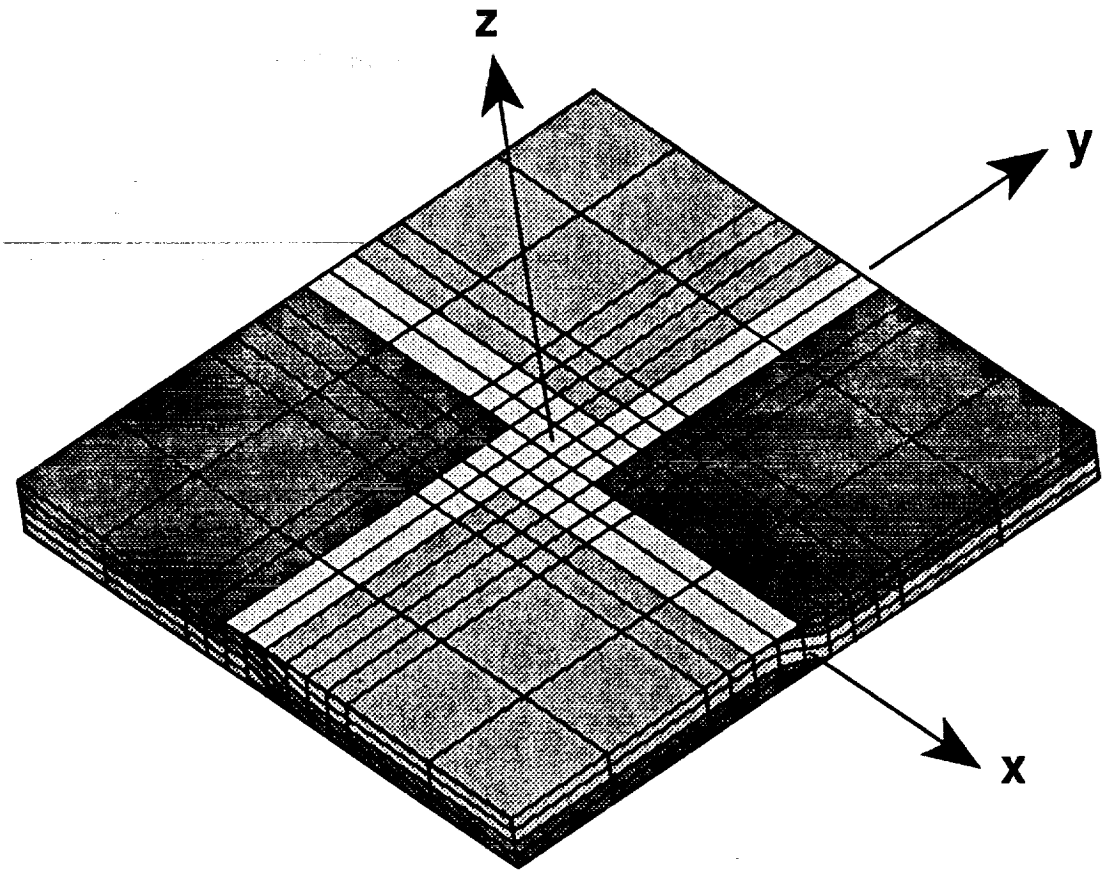

(b) Refined mesh (3793 nodes, 768 elements)

Figure 3. Concluded.

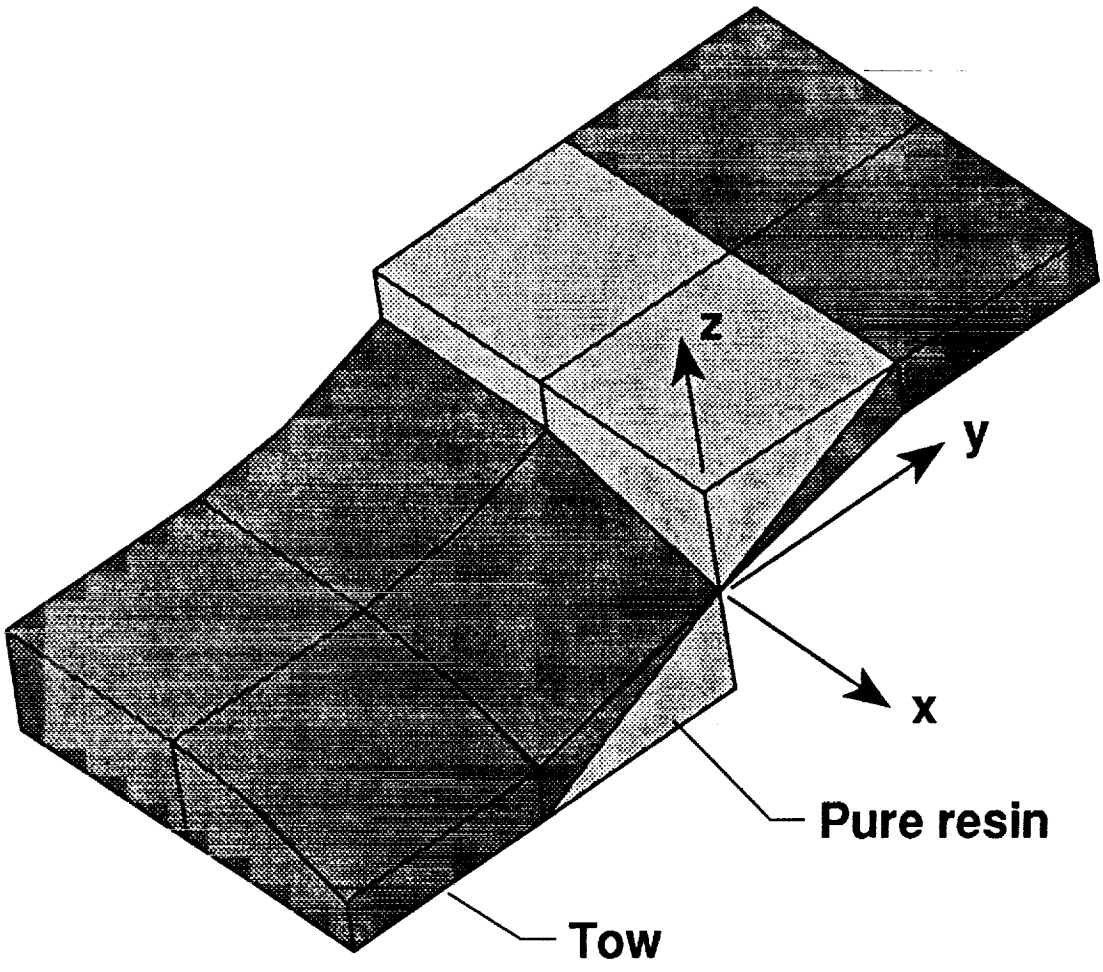

Figure 4. Basic element group used to generate mesh.

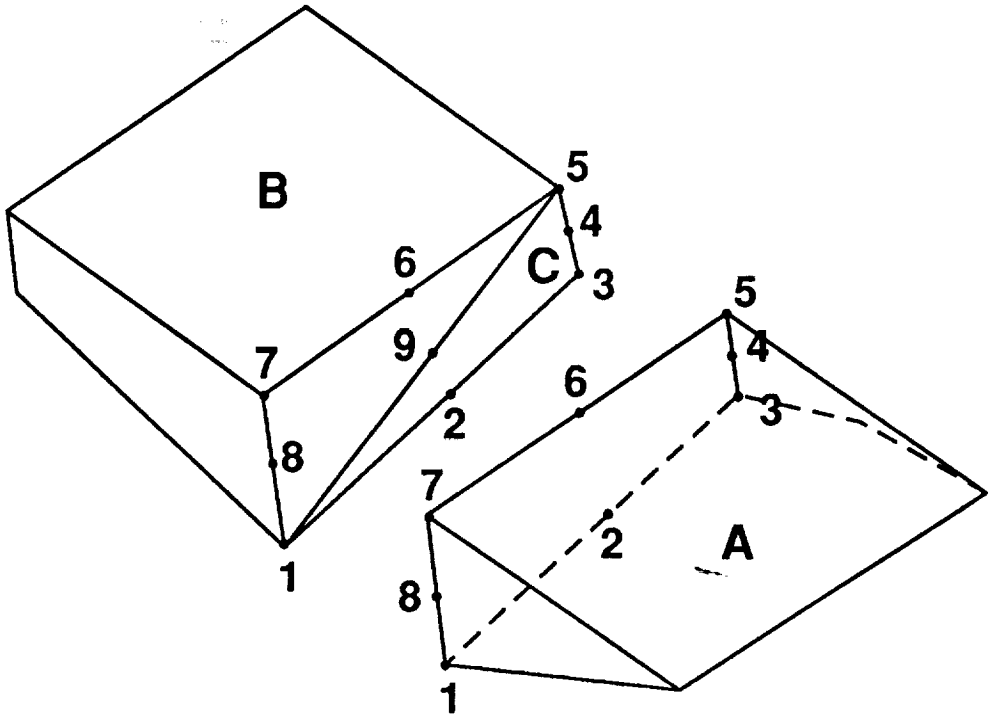

Figure 5. Close-up of elements A and B from Figure 3a. Elements are seperated to show incompatability.

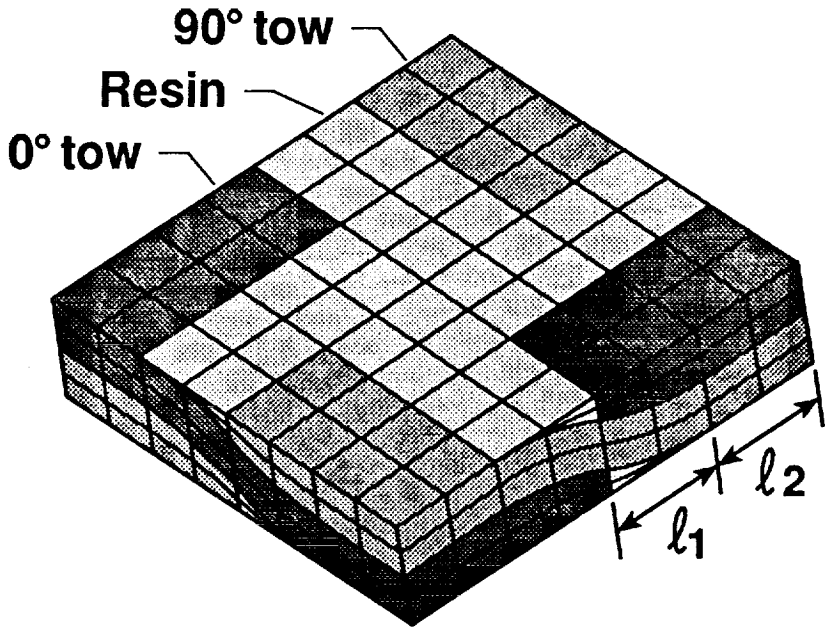

Figure 6. Mesh with large waviness ratio.

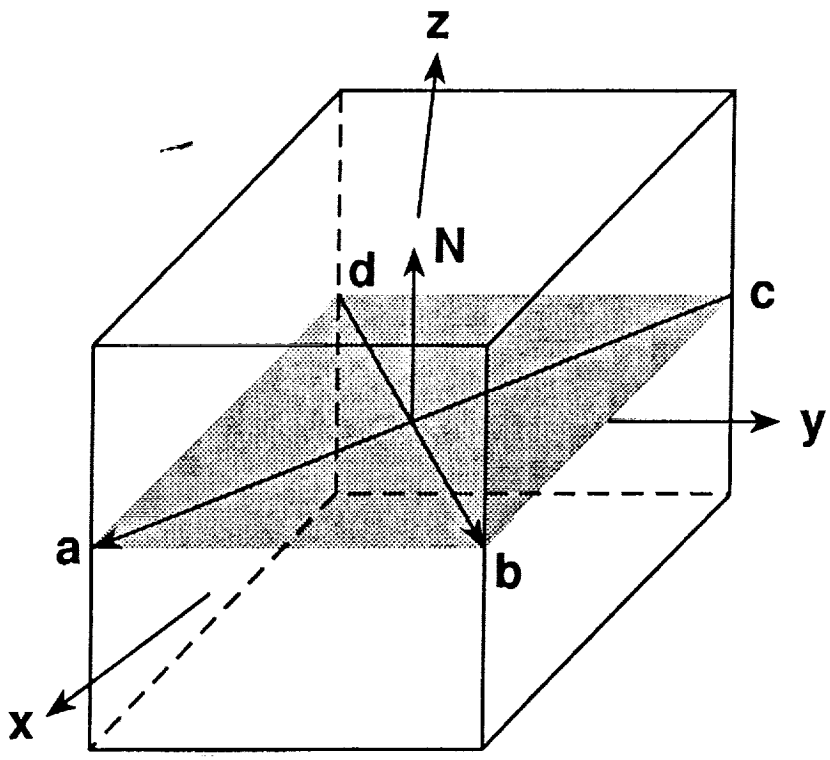

Figure 7. Calculation of element orientation.

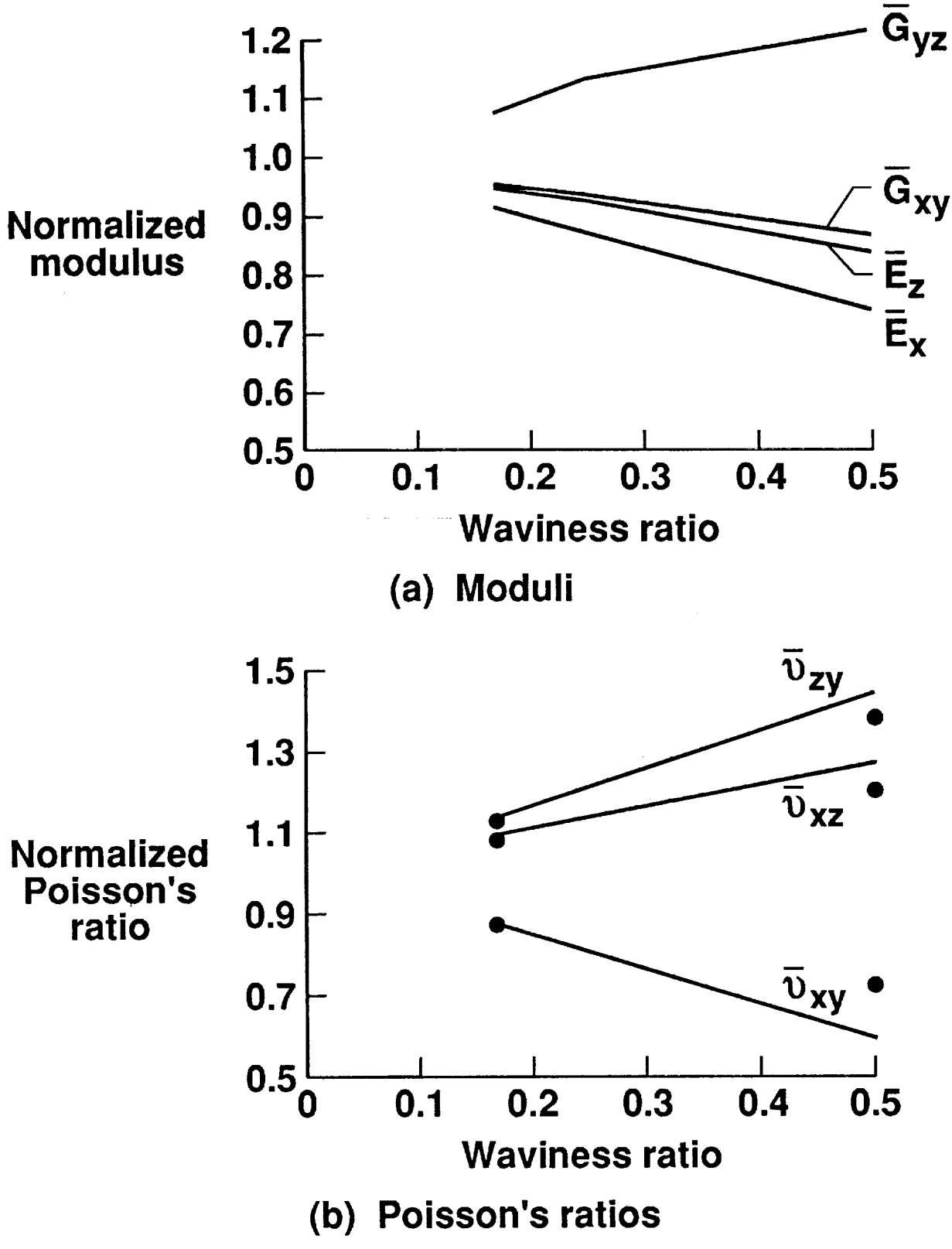

Figure 8. Effect of waviness on moduli and Poisson's ratio.

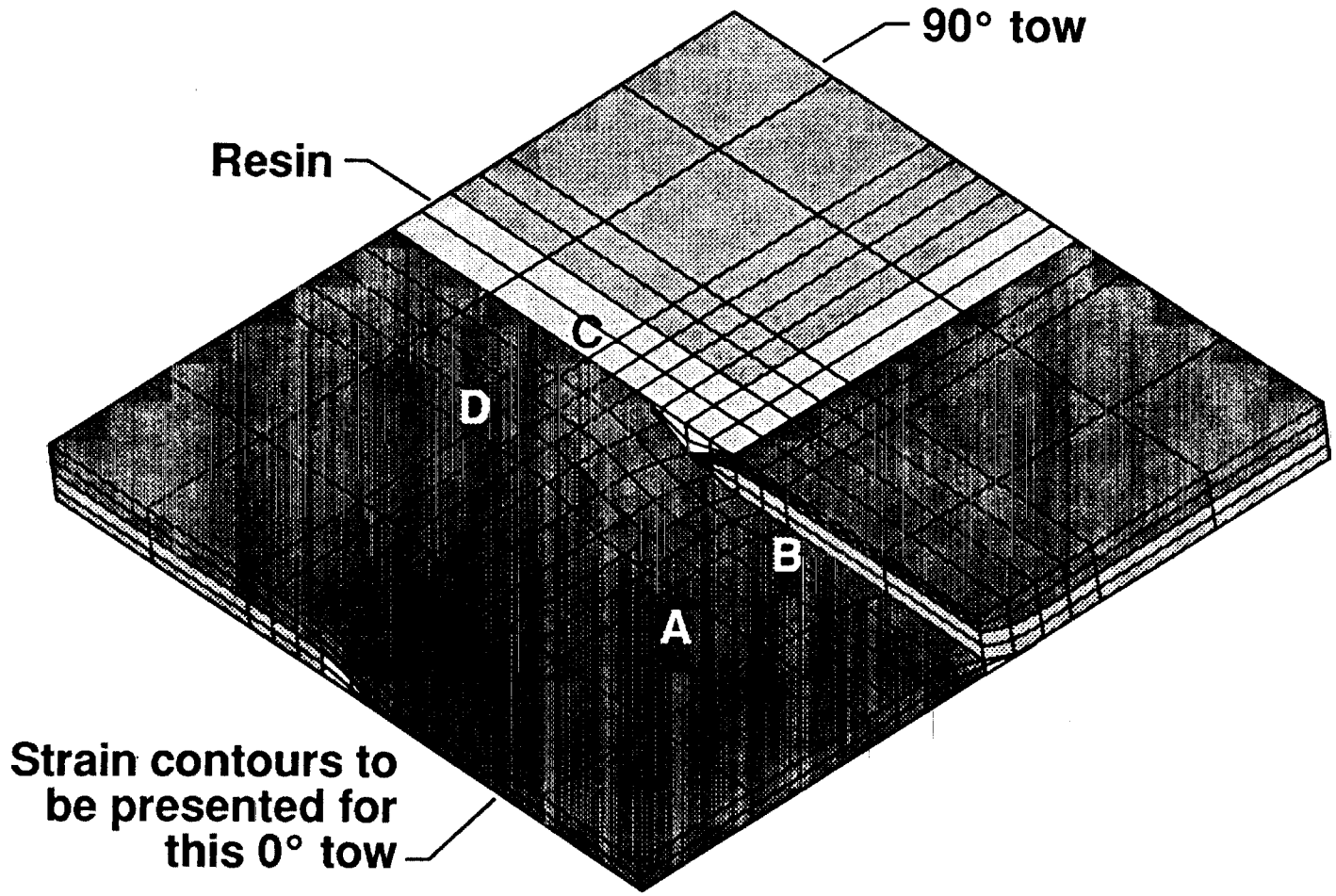

Figure 9. Identification of area for which strain contours will be presented. Waviness ratio = .167.

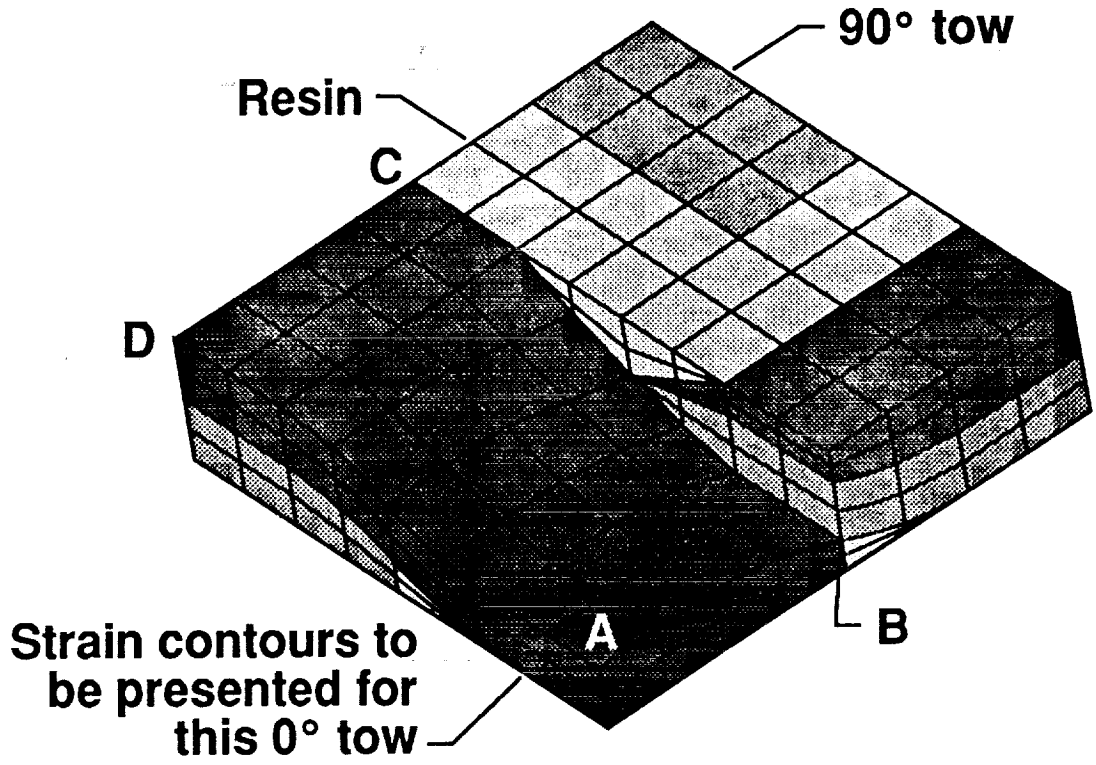

Figure 10. Identification of area for which strain contours will be presented. Waviness ratio = .5.

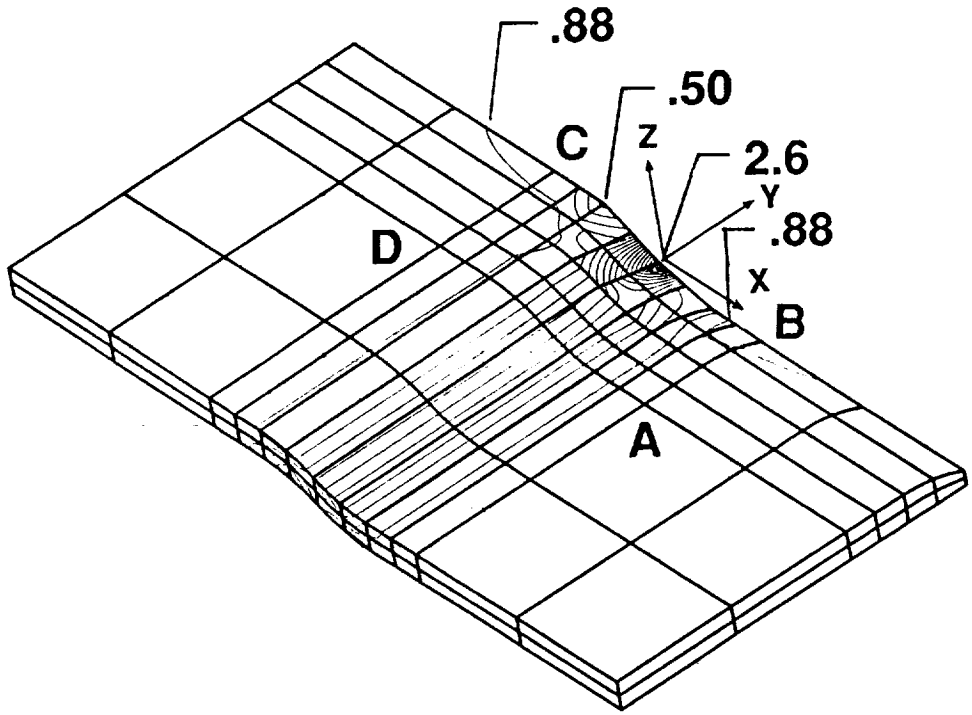

Figure 11. Normalized axial strain, $\varepsilon_1/\varepsilon_x^o$.

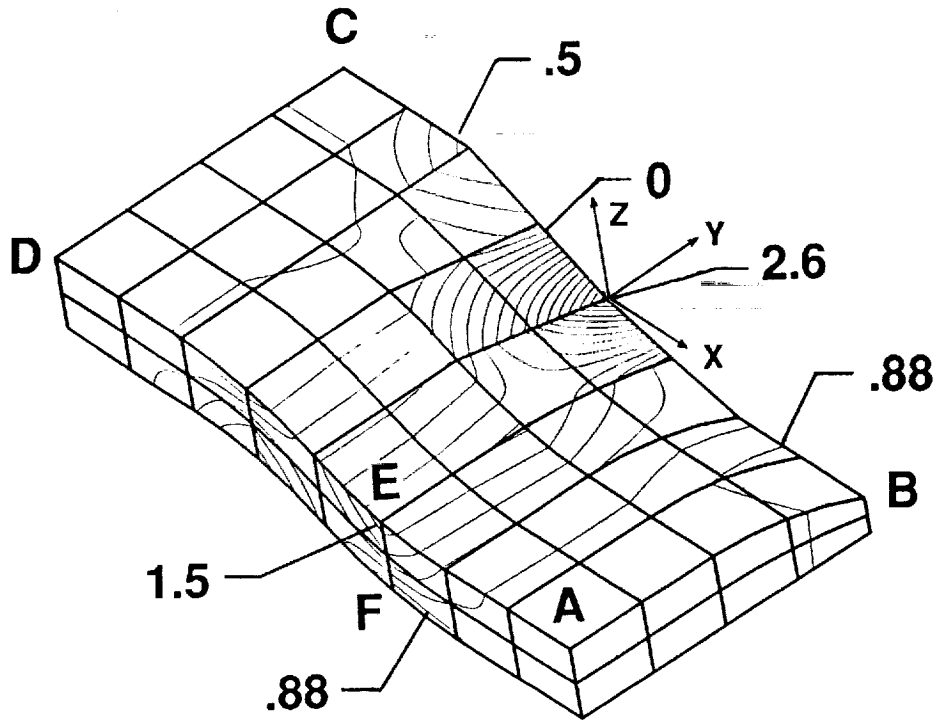

(a) $\varepsilon_1/\varepsilon_x^o$.

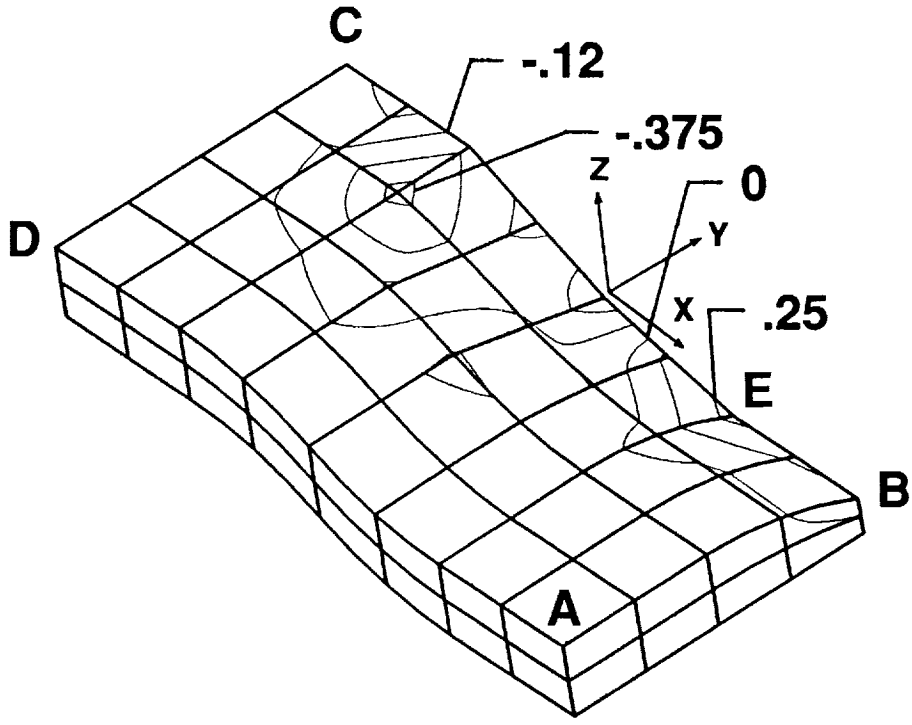

(b) $\varepsilon_2/\varepsilon_x^o$.

Figure 12. Normalized strain contours for 0^o tow. Waviness ratio = .167.

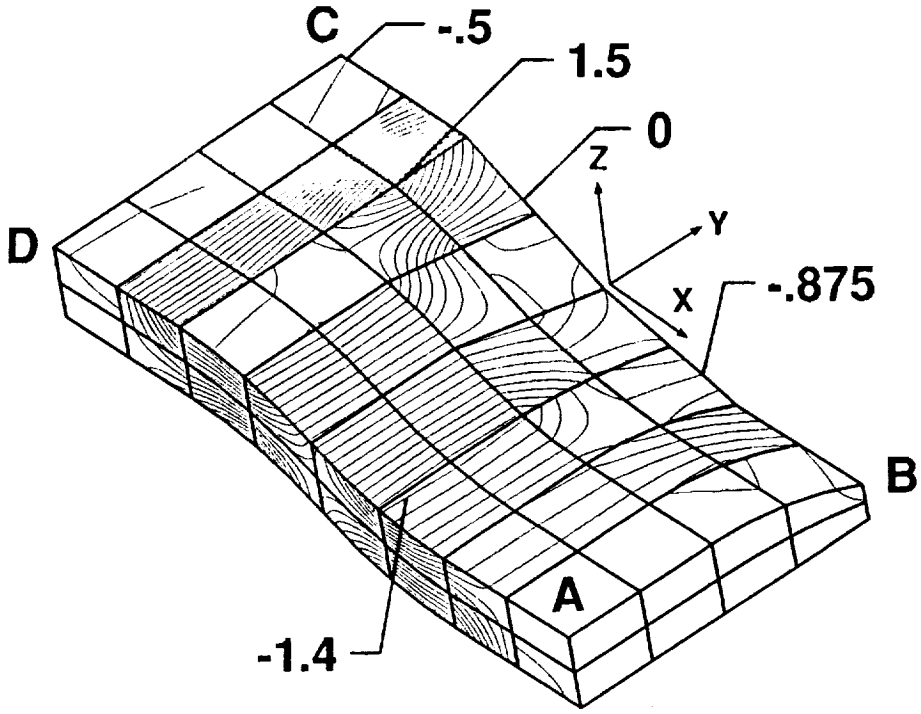

(c) $\varepsilon_3/\varepsilon_x^o$.

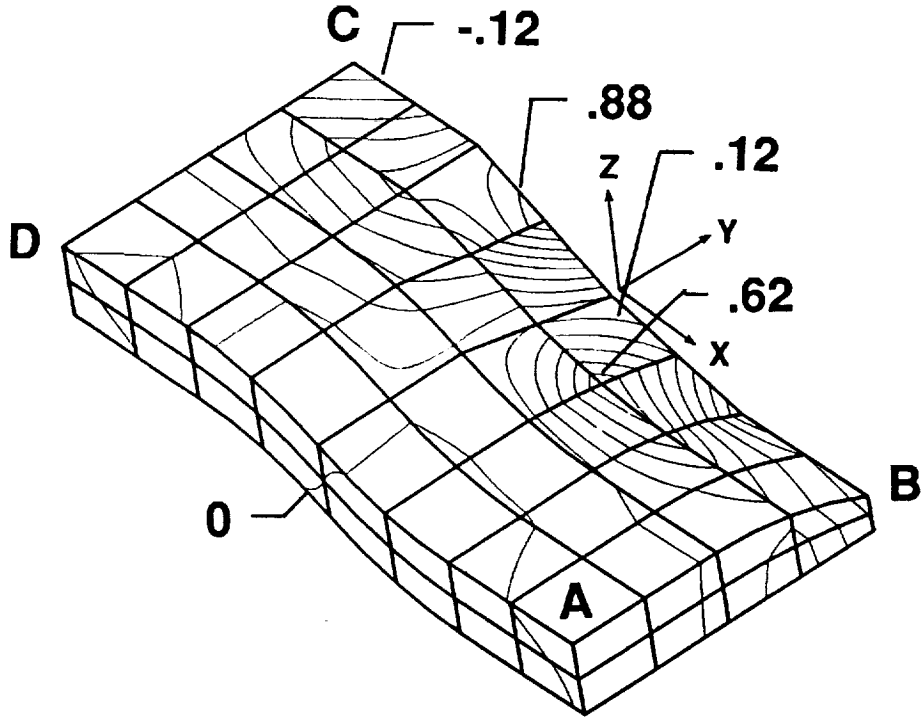

(d) $\varepsilon_{12}/\varepsilon_x^o$.

Figure 12. Continued.

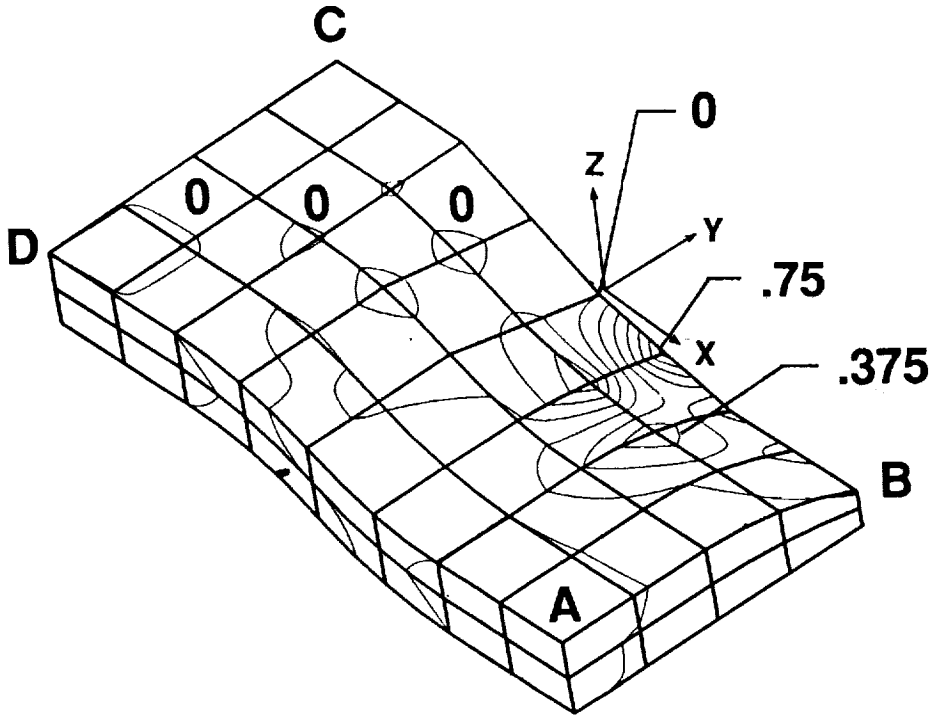

(e) $\varepsilon_{23}/\varepsilon_x^o$.

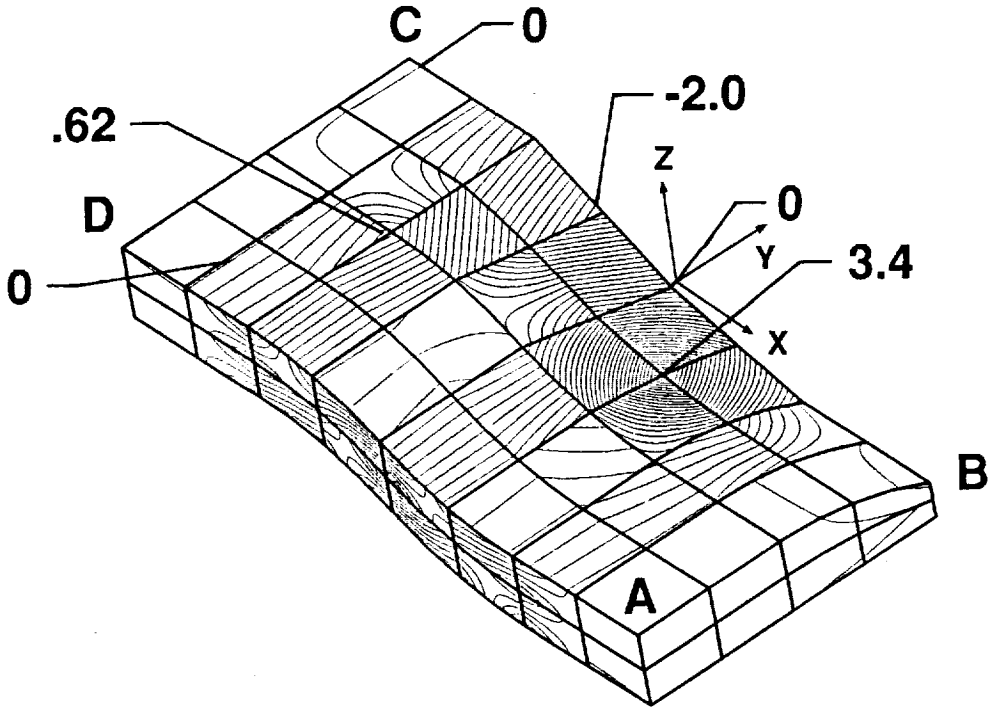

(f) $\varepsilon_{13}/\varepsilon_x^o$.

Figure 12. Concluded.

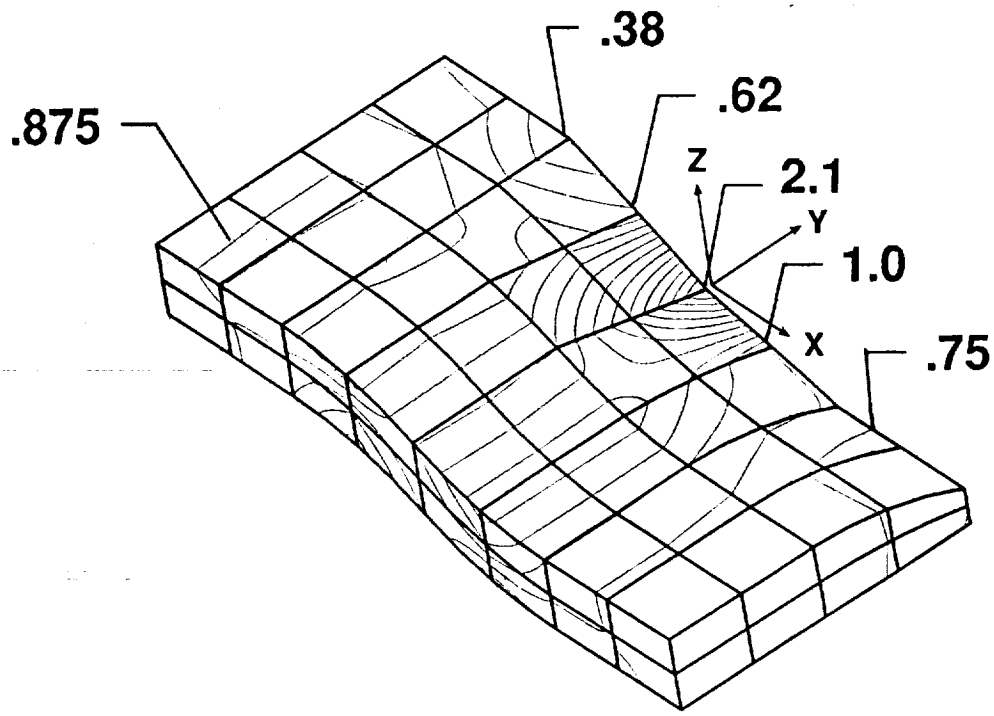

(a) $\varepsilon_1/\varepsilon_x^o$.

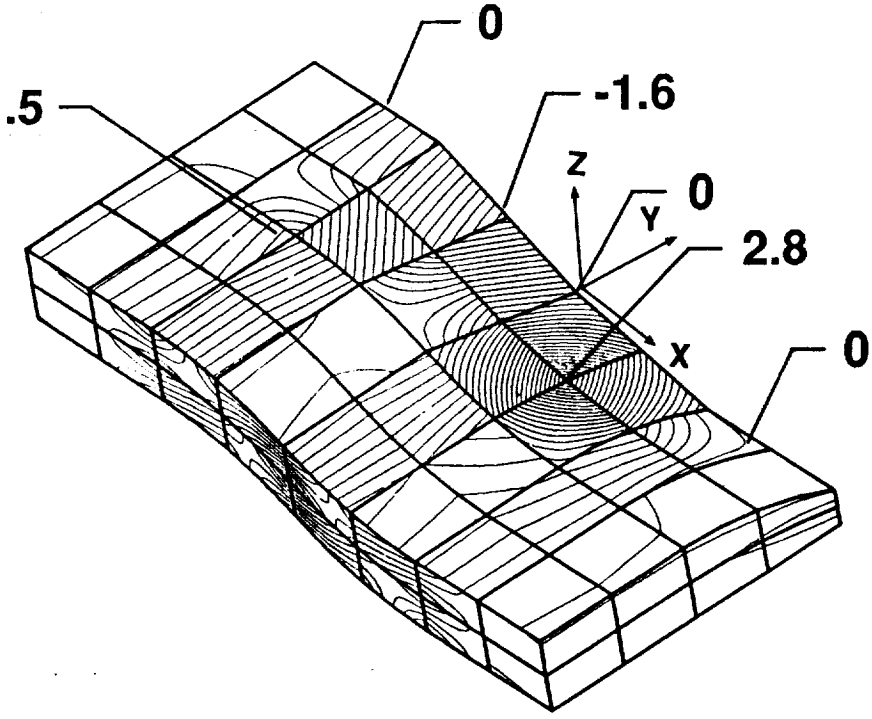

(b) $\varepsilon_{13}/\varepsilon_x^o$.

Figure 13. Normalized strain contours for 0^o tow. Waviness ratio = .5.

NASA
National Aeronautics and Space Administration

Report Documentation Page

1. Report No.	2. Government Accession No.	3. Recipient's Catalog No.
NASA TM-101672		

4. Title and Subtitle	5. Report Date
Three-Dimensional Stress Analysis of Plain Weave Composites	November 1989
	6. Performing Organization Code
7. Author(s)	8. Performing Organization Report No.
John D. Whitcomb	
9. Performing Organization Name and Address	10. Work Unit No.
NASA Langley Research Center Hampton, VA 23665-5225	505-63-01-05
	11. Contract or Grant No.
12. Sponsoring Agency Name and Address	13. Type of Report and Period Covered
National Aeronautics and Space Administration Washington, DC 20546-0001	Technical Memorandum
	14. Sponsoring Agency Code

15. Supplementary Notes

16. Abstract

Techniques were developed and described for performing three-dimensional finite element analysis of plain weave composites. This paper emphasizes aspects of the analysis which are different from analysis of traditional laminated composites, such as the mesh generation and representative unit cells. The analysis was used to study several different variations of plain weaves which illustrate the effects of tow waviness on composite moduli, Poisson's ratios, and internal strain distributions. In-plane moduli decreased almost linearly with increasing tow waviness. The tow waviness was shown to cause large normal and shear strain concentrations in composites subjected to uniaxial load. These strain concentrations may lead to earlier damage initiation than occurs in traditional cross-ply laminates.

17. Key Words (Suggested by Authors(s))	18. Distribution Statement
Composites Weaves Stress Analysis 3D composites	Unclassified–Unlimited Subject Category 24

19. Security Classif. (of this report)	20. Security Classif. (of this page)	21. No. of Pages	22. Price
Unclassified	Unclassified	32	A03

NASA FORM 1626 OCT 86
For sale by the National Technical Information Service, Springfield, Virginia 22161-2171